DMD Fast Forward. Published on February 21, 2018 as DOI: 10.1124/dmd.117.078881
This article has not been copyedited and formatted. The final version may differ from this version.

Hepatic transport of 25-hydroxyvitamin D_3 conjugates: a mechanism of 25-hydroxyvitamin D_3 delivery to the intestinal tract

Chunying Gao, Michael Z. Liao, Lyrialle W. Han, Kenneth E. Thummel, and Qingcheng Mao*

Department of Pharmaceutics, School of Pharmacy, University of Washington, Seattle, Washington 98195, United States

Running title: Transport of 25-hydroxylvitamin D_3 conjugates

***Corresponding author:**

Qingcheng Mao, Ph.D.
Department of Pharmaceutics
University of Washington
Seattle, WA 98195-7610
Phone: (206) 685-0355
Email: qmao@uw.edu

Number of text pages: 44
Number of tables: 1
Number of figures: 9
Number of references: 42
Number of words in the Abstract: 248
Number of words in the Introduction: 738
Number of words in the Discussion: 1541

Abbreviations: BCRP, breast cancer resistance protein; CYP, cytochrome P450; FTC, the BCRP inhibitor fumitremorgin C; CsA, cyclosporine A, HBSS, Hank's balanced salt solution; MRP2, multidrug resistance protein 2; MRP3, multidrug resistance protein 3; MRP4, multidrug resistance protein 4; OATP1B1, organic anion transporting polypeptide 1B1; OATP1B3, organic anion transporting polypeptide 1B3; OATP2B1, organic anion transporting polypeptide 2B1; VDR, vitamin D receptor; DBP, vitamin D binding protein; 25OHD$_3$, 25-hydroxyvitamin D_3; 1α,25-(OH)$_2$D$_3$, 1α,25-dihydroxyvitamin D_3; 25OHD$_3$-S, 25OHD$_3$-3-*O*-sulfate; 25OHD$_3$-G, 25OHD$_3$-3-*O*-glucuronide; SCHH, sandwich cultured human hepatocyte; E_1-3-S, estrone-3-sulfate; E_2-3-S, estradiol-3-sulfate; E_2-17β-G, estradiol-17β-glucuronide; DAPTAD, 4-(4'-dimethylaminophenyl)-1,2,4-triazoline-3,5-dione; PAPS,

3'-phosphoadenosine-5'-phosphosulfate; LC-MS/MS, Liquid chromatography-tandem mass spectrometry; HEK293, human embryonic kidney 293 cell line; BEI, Biliary efflux index

DMD Fast Forward. Published on February 21, 2018 as DOI: 10.1124/dmd.117.078881
This article has not been copyedited and formatted. The final version may differ from this version.

ABSTRACT

Vitamin D_3 is an important prohormone critical for maintaining calcium and phosphate homeostasis in the body and regulating drug-metabolizing enzymes and transporters. $25OHD_3$, the most abundant circulating metabolite of vitamin D_3, is further transformed to the biologically active metabolite $1\alpha,25\text{-}(OH)_2D_3$ by CYP27B1 in the kidney and extra-renal tissues, and to non-active metabolites by other CYP enzymes. In addition, $25OHD_3$ undergoes sulfation and glucuronidation in the liver, forming two major conjugative metabolites, $25OHD_3$-3-*O*-sulfate ($25OHD_3$-S) and $25OHD_3$-3-*O*-glucuronide ($25OHD_3$-G), both of which were detected in human blood and bile. Considering that the conjugates excreted into the bile may be circulated to and reabsorbed from the intestinal lumen, deconjugated to $25OHD_3$ and then converted to $1\alpha,25\text{-}(OH)_2D_3$, exerting local intestinal cellular effects, it is crucial to characterize enterohepatic transport mechanisms of $25OHD_3$-S and $25OHD_3$-G, and thereby understand and predict mechanisms of inter-individual variability in mineral homeostasis. In the present study, with plasma membrane vesicle and cell-based transport studies, we showed that $25OHD_3$-G is a substrate of MRP2, MRP3, OATP1B1 and OATP1B3, and that $25OHD_3$-S is likely a substrate of BCRP, OATP2B1 and OATP1B3. We also demonstrated sinusoidal and canalicular efflux of both conjugates using sandwich cultured human hepatocytes. Given substantial expression of these transporters in liver hepatocytes and intestinal enterocytes, this study demonstrates for the first time that transporters could play important roles in the enterohepatic circulation of $25OHD_3$ conjugates, providing an alternative pathway of $25OHD_3$ delivery to the intestinal tract, which

could be critical for vitamin D receptor-dependent gene regulation in enterocytes.

DMD Fast Forward. Published on February 21, 2018 as DOI: 10.1124/dmd.117.078881
This article has not been copyedited and formatted. The final version may differ from this version.

INTRODUCTION

Vitamin D_3 is essential for regulation of calcium and phosphate homeostasis in the body. Vitamin D_3 exerts most of its biological functions through a biologically active metabolite, 1α,25-$(OH)_2D_3$, which binds with high affinity to vitamin D receptor (VDR) and activates transcription of target genes (Christakos, 2012). Besides regulating intestinal absorption of calcium and phosphate, VDR signaling also appears to be important for regulation of human intestinal CYP3A4 expression (Thummel et al., 2001), which has been shown to be associated with seasonal changes in vitamin D production (Thirumaran et al., 2012) and can be modified by vitamin D supplementation (Schwartz, 2009).

The biologically active metabolite 1α,25-$(OH)_2D_3$ is generated following two metabolic steps (Fig. 1). First, 25OHD_3 is produced from vitamin D_3 primarily by hepatic CYP2R1. 25OHD_3, which is the major circulating form of vitamin D_3 (Henry and Norman, 1984), tightly binds to plasma proteins (e.g., vitamin D binding protein, DBP) and exhibits a relatively long (~14 d) plasma half-life, and therefore is used as a biomarker for vitamin D exposure (Holick, 2007). 25OHD_3 is then further metabolized to 1α,25-$(OH)_2D_3$ primarily by CYP27B1 in the kidney and certain extra-renal tissues (Hewison et al., 2007; Feldman et al., 2014).

Although the kidney is generally regarded to be the main source of 1α,25-$(OH)_2D_3$, CYP27B1 is also expressed in a number of extra-renal tissues, including intestinal epithelial cells (Bikle, 2009; Bikle, 2014). Importantly, as suggested by Balesaria et al. (Balesaria et al., 2009) and others (Bises et al., 2004), 1α,25-$(OH)_2D_3$-mediated biological effects in the intestine might

DMD Fast Forward. Published on February 21, 2018 as DOI: 10.1124/dmd.117.078881
This article has not been copyedited and formatted. The final version may differ from this version.

also be produced via an intracrine process involving the bioactivation of $25OHD_3$ by intestinal CYP27B1. A recent study provided direct experimental evidence that CYP27B1 in duodenum indeed can metabolize $25OHD_3$ and contribute to local $1\alpha,25\text{-}(OH)_2D_3$ production in the intestine (Gawlik et al., 2015). However, the delivery of $25OHD_3$ to the intestinal mucosal cells remains unclear, but could involve production and delivery of vitamin D_3 conjugates.

Studies in humans using radioactive compounds suggested that vitamin D_3 and its hydroxylated metabolites are excreted through the bile in the forms of conjugates (Avioli et al., 1967). In one study, $25OHD_3$ was suggested to go through extensive enterohepatic circulation, where 85% of secreted radioactivity into duodenum was reabsorbed in 24 h after intravenous administration of $[^3H]$-$25OHD_3$ (Arnaud et al., 1975). Considering the wide distribution of β-glucuronidase (Whiting et al., 1993; Oleson and Court, 2008) and steroid sulfatase (Miki et al., 2002) in intestinal bacteria and within the enterocyte, conjugated $25OHD_3$ in the bile may be reabsorbed from the intestinal lumen in intact form or as an aglycone after hydrolysis by enzymes or bacteria in the intestinal tract.

In addition to 1α-hydroxylation, $25OHD_3$ undergoes a series of catabolic hydroxylation reactions (e.g., 23S, 24R and 4β) that mediate inactivation of vitamin D_3 and its excretion (Christakos et al., 2010; Wang et al., 2012). $25OHD_3$ also undergoes sulfation and glucuronidation in the liver, generating two major circulating conjugative metabolites, $25OHD_3$-3-*O*-sulfate ($25OHD_3$-S) (Wong et al., 2018) and $25OHD_3$-3-*O*-glucuronide ($25OHD_3$-G) (Wang et al., 2014) (Fig. 1). In healthy humans, plasma concentrations can reach as

DMD Fast Forward. Published on February 21, 2018 as DOI: 10.1124/dmd.117.078881
This article has not been copyedited and formatted. The final version may differ from this version.

high as 185 nM for $25OHD_3$, 100 nM for $25OHD_3$-S, and 10 nM for $25OHD_3$-G (Gao et al., 2017). Both conjugative metabolites are tightly bound to DBP, with an affinity similar to that of $25OHD_3$, and were not detected in the urine of healthy individuals. The high protein binding of vitamin D_3 conjugates in the blood not only reduces urinary excretion from the body, but also greatly limits the passive diffusion and active transport across membrane barriers, and thus minimizing the delivery of unbound vitamin D-derived conjugates to target tissues (e.g., intestinal epithelia) in the body. In contrast, due to the absence of binding proteins in the bile, biliary conjugates of vitamin D_3 should be directly accessible to the intestinal epithelia cells and uptake transporters for hormone conjugates (Hofmann, 2011). We hypothesized that $25OHD_3$ conjugates excreted into the bile are deconjugated by bacterial or intracellular sulfatase and glucuronidase and then hydroxylated by intestinal CYP27B1 to $1\alpha,25\text{-}(OH)_2D_3$, thereby regulating VDR target gene expression.

To test the hypothesis that the regulation of intestinal VDR target genes is mediated in part by $1\alpha,25\text{-}(OH)_2D_3$ in the intestinal tract, it is essential to understand the hepatic and intestinal transport of conjugative $25OHD_3$ metabolites. However, to date, there is essentially nothing known about these processes. The objective of the current study was to characterize the major uptake and efflux transport mechanisms for $25OHD_3$-S and $25OHD_3$-G in the liver.

MATERIALS and METHODS

Materials. Ko143, MK571, indomethacin, rifampin, cyclosporine A (CsA), fumitremorgin C,

cholic acid, taurocholate, estrone-3-sulfate (E_1-3-S), estradiol-17β-glucuronide (E_2-17β-G), estradiol-3-sulfate (E_2-3-S), 3'-phosphoadenosine-5'-phosphosulfate (PAPS), adenosine 5'-triphosphate (ATP) disodium salt, adenosine 5'-monophosphate (AMP) monohydrate and glutathione were purchased from Sigma-Aldrich (St. Louis, MO). 25OHD$_3$, d_6-25OHD$_3$, 25OHD$_3$-S and 25OHD$_3$-G were obtained from Toronto Research Chemicals (Toronto, Canada). Hygromycin B, G-418 and RIPA lysis buffer were purchased from Fisher Scientific (Thermo Fisher, Waltham, MA). All other buffers and chemicals were of the highest grade commercially available.

Cell culture medium, antibiotic-antimycotic solution (100 ×) and Hank's balanced salt solution (HBSS) were purchased from Invitrogen (Carlsbad, CA). Fetal bovine serum (FBS) was obtained from VWR (Radnor, PA). Plasma membrane vesicles including Sf9 cell-overexpressing BCRP, MRP2 or MRP3, HEK293 cell-overexpressing MRP4 and their corresponding control membrane vesicles were purchased from SOLVO Biotechnology (Szeged, Hungary). Flp-In-Chinese Hamster Ovary (CHO)/OATP2B1, Flip-In-CHO mock, CHO/OATP1B1, CHO/OATP1B3 and wild-type CHO cells were provided by Dr. Bruno Stieger of the Department of Clinical Pharmacology and Toxicity, University Hospital Zurich, Switzerland, through Dr. Bruno Hagenbuch of the Department of Pharmacology, Toxicology and Therapeutics, University of Kansas Medical Center. Pre-plated sandwich cultured human hepatocytes (SCHHs) were obtained from IVAL (Malden, MA). Multiscreen™ HTS Vacuum Manifold and 96-well filter plates with glass fiber filters were purchased from Merck Millipore (Billerica, MA).

DMD Fast Forward. Published on February 21, 2018 as DOI: 10.1124/dmd.117.078881
This article has not been copyedited and formatted. The final version may differ from this version.

Ultracentrifuge tubes (Beckman 343775) for unbound fraction determination were purchased from Beckman Coulter (Brea, CA). Anonymous, pooled human bile was kindly provided by Dr. Evan D. Kharasch at the Washington University in St. Louis (St. Louis, MO).

Human Bile Analysis. Pooled human bile from different donors was analyzed with a sensitive LC-MS/MS method coupled with derivatization (Gao et al., 2017), and deuterated internal standards (d_6-25OHD$_3$-S and d_6-25OHD$_3$-G) used in the analysis were obtained through biotransformation from d_6-25OHD$_3$ as previously described(Gao et al., 2012b). In brief, human bile (100 µl) was spiked with d_6-25OHD$_3$-S and d_6-25OHD$_3$-G and was then precipitated with 200 µl acetonitrile. The resulting supernatant was buffered with 1 ml of 0.1 M sodium acetate (pH 3.2) and subjected to solid-phase extraction (SPE) using the Waters Oasis WAX (60 mg, 3 cc) anion exchange cartridges. Eluates from the SPE columns were then dried and reconstituted in 10 µl of methanol and derivatized with 4-(4'-dimethylaminophenyl)-1,2,4-triazoline-3,5-dione (DAPTAD) for 1 h at room temperature in the dark. The reaction mixture was evaporated under N_2 flow and reconstituted in 100 µl of mobile phase. A centrifugation step (13,362 × *g* for 5 min) was applied to remove insoluble materials prior to LC-MS/MS analysis. DAPTAD-25OHD$_3$-S, DAPTAD-d_6-25OHD$_3$-S, DAPTAD-25OHD$_3$-G and DAPTAD-d_6-25OHD$_3$-G were analyzed using an AB Sciex QTRAP 6500 LC-MS/MS system. Due to the lack of blank bile matrix, calibration curves were plotted with corrected peak area ratios of DAPTAD-25OHD$_3$-S/G and DAPTAD-d_6-25OHD$_3$-S/G by subtracting “blank” samples from those spiked with serial

$25OHD_3$-S and $25OHD_3$-G solutions.

Inside-out Membrane Vesicular Uptake Assay. A rapid filtration technique modified from a previously reported method (Gao et al., 2012a) was used for inside-out plasma membrane vesicular transport assays. In brief, plasma membrane vesicles (25 μg protein) and test compounds of various concentrations were incubated at 37ºC in the presence of ATP or AMP (5 mM) in a buffer (pH 7.0) containing 10 mM Tris/HCl, 10 mM $MgCl_2$, 250 mM sucrose for HEK293 membrane vesicles or in a buffer (pH 7.0) containing 40 mM MOPS/Tris, 70 mM KCl and 7.5 mM $MgCl_2$ for Sf9 plasma membrane vesicles. Glutathione (2 mM) was added to the incubations for MRP transporters. Transport was terminated after incubation for a designated time by the addition of 200 μL of ice-cold buffer (containing 1.5% BSA, for $25OHD_3$-S and $25OHD_3$-G). The mixture was rapidly transferred to a 96-well glass fiber filter plate and then washed five times with 200 μL of ice-cold wash buffer (containing 1.5% BSA, for $25OHD_3$-S and $25OHD_3$-G). The compound trapped in membrane vesicles was retained on the filters and eluted by the addition of 200 μL of methanol containing corresponding internal standard. E_2-17β-G, a known substrate of MRPs and BCRP, was used as a positive control for MRPs and BCRP or a probe substrate of these transporters. In inhibitory studies using E_2-17β-G as a probe substrate, E_2-17β-G at 10 μM (for BCRP and MRP4) or 2 μM (for MRP2 and MRP3) were incubated with transporter-overexpressing membrane vesicles (25 μg) in the presence of varying concentrations of $25OHD_3$-S. The incubations were conducted and terminated under the same

conditions as described above. Vehicle (DMSO) used to dissolve test compounds was kept below 0.2% (v/v) in all the incubations and no effects of the vehicle at concentrations below 0.2% (v/v) on vesicular uptake or non-specific binding of 25OHD$_3$-S and 25OHD$_3$-G were observed. ATP-dependent uptake of 25OHD$_3$-S, 25OHD$_3$-G and E$_2$-17β-G into inside-out plasma membrane vesicles was calculated by subtracting the uptake in the presence of AMP from that in the presence of ATP.

Unbound Fractions of 25OHD$_3$-S and 25OHD$_3$-G in Plasma Membrane Vesicle Incubations. Ultracentrifugation was used to determine unbound fraction of 25OHD$_3$-S and 25OHD$_3$-G in incubation buffers of membrane vesicular transport assays as previously described (Shirasaka et al., 2013). Briefly, 25OHD$_3$-S or 25OHD$_3$-G at various concentrations was incubated with mock Sf9 or HEK293 membrane vesicles in ultracentrifuge tubes (Beckman 343775) under the same experimental conditions as the vesicular transport assays (e.g., temperature and incubation time). After incubation, the mixture was centrifuged at 435,000 × *g* at 37 °C for 90 min using a Sorval Discovery M150 SE ultracentrifuge and a Thermo Scientific S100-AT3 rotor (Waltham, MA). The unbound fraction (%) was calculated by dividing the concentration of 25OHD$_3$-S or 25OHD$_3$-G in the supernatant after centrifugation by the total concentration in a parallel mixture incubated at 37 °C for 90 min without centrifugation.

Culture of OATP-overexpressing Cells. Cells were maintained at 37 °C in a humidified 5%

CO_2 incubator. Flp-In-CHO cells transfected with OATP2B1 (Flp-In-CHO/OATP2B1) and mock control cells were cultured as previously described (Pacyniak et al., 2010). In brief, cells were maintained in F-12 Nutrient Mixture containing 10% fetal bovine serum, 2 mM L-glutamine, 100 U/mL penicillin, 100 µg/mL streptomycin, 0.25 µg/mL amphotericin B, and 400 µg/ml hygromycin B. CHO cells stably expressing OATP1B1 (CHO/OATP1B1) and OATP1B3 (CHO/OATP1B3) were cultured in phenol-red free, low glucose DMEM media with 10% FBS, 100 U/mL penicillin, 100 µg/mL streptomycin, 0.25 µg/mL amphotericin B, and 50 µg/ml L-proline in the presence of 500 µg/ml G418 as previously described (Gui et al., 2010). Wild-type (WT) CHO parent cells were cultured in the same media as above without G418.

Cellular Uptake Transport Assay. OATP-transfected CHO cells and respective control cells were seeded on CELLCOAT® 24-well plates (Greiner Bio-One, Monroe, NC) at a density of approximately 4×10^4 cells/well. For CHO/OATP1B1, CHO/OATP1B3 and wild-type CHO parent control cells, after cells were plated and cultured for 24 h, 5 mM Na-butyrate was added into culture medium and the culture was continued for another 24 h to induce OATP expression. Flp-In-CHO/OATP2B1 and mock control CHO cells were cultured in media without Na-butyrate for 48 h straight. Prior to uptake experiments, cells were washed and equilibrated in HBSS at 37ºC for 10 min. Uptake was initiated by adding 0.5 ml of HBSS containing 25OHD_3-S or 25OHD_3-G at various concentrations to corresponding cells and terminated after incubation for 5 min at 37ºC by aspirating incubation buffer and washing the cells twice with 2 ml of ice-cold

fresh HBSS (containing 1.5% BSA, for 25OHD$_3$-S and 25OHD$_3$-G). An aliquot of 50 µl of the uptake incubation buffer was collected for each concentration to determine free concentrations of 25OHD$_3$-S or 25OHD$_3$-G in the incubation buffers. After the uptake, cells were lysed with 0.25 ml of methanol containing corresponding internal standard and centrifuged at 13,362 × g for 5 min. The supernatant was then evaporated and reconstituted in 100 µl of mobile phase for LC-MS analysis. In parallel, cells grown under the same conditions were lysed with 0.25 ml of RIPA cell lysis buffer and protein concentrations of cell lysates were determined using Pierce BCA protein assay kit (Pierce Chemical, Rockford, IL). Accumulation (or uptake) of 25OHD$_3$-S or 25OHD$_3$-G in cells was normalized to protein content of the cells. For positive control, transport of E_2-17β-G (OATP1B1 and OATP1B3) and E_1-3-S (OATP2B1) was conducted at 10 µM under the same conditions as described above.

Data Analysis for Uptake Assays. All the membrane vesicular and cellular uptake experiments were performed in triplicate or quadruplicate and with at least two independent repeats. Differences in membrane vesicular uptake between ATM and AMP or in cellular accumulation between OATP expressing and control cells were analyzed using unpaired Student's *t*-test. Differences with p value of < 0.05 were considered statistically significant. K_m and V_{max} of transport kinetics were estimated by fitting of experimental data to the Michaelis-Menten equation with nonlinear regression. IC_{50} values were also determined by nonlinear regression as previously described (Duan et al., 2015). All the analyses were performed using the GraphPad

Prism software (GraphPad Prism 5.01, La Jolla, CA).

Efflux of 25OHD$_3$-S or 25OHD$_3$-G from Sandwich Cultured Human Hepatocytes. SCHHs were obtained from five female donors (HH1055, HH1085, HH1007 and HH1103) and one male donor (HH1031). SCHHs were plated in 96-well plates on day 1 by the vendor and shipped with 37°C heating patches overnight on day 2. Upon arrival of cells, the culture media were replaced with fresh and warm hepatocyte maintenance media provided by the vendor and the cells were cultured for another 2 days with medium change every day. On day 5, cells were washed and pre-incubated in HBSS with 25OHD$_3$ at 10 µM for 4 h and efflux was initiated by washing and incubating cells with 100 µl of fresh HBSS buffer with or without calcium. Human vitamin D binding protein (DBP) was added to incubation buffer to 3 µM during the efflux phase to reduce non-specific binding of 25OHD$_3$ conjugates (e.g., to cell membrane and plastic cell culture flask). To confirm if efflux transporters are involved in the canalicular and sinusoidal efflux of 25OHD$_3$-S and 25OHD$_3$-G, the BCRP inhibitor FTC (10 µM) or the MRP inhibitor MK571 (40 µM) was added in incubation buffer, throughout the 4-h loading and 20-min efflux phases. As a positive control, SCHHs were loaded with 2 µM taurocholate for 20 min, and the efflux was initiated by washing and incubating the cells with fresh HBSS with or without calcium. During the efflux phase, incubation buffer (100 µl) was collected at designated time points from corresponding wells which were loaded with 25OHD$_3$ or taurocholate. The cells were lysed with 100 µl methanol and collected at the end of the efflux phase. For 25OHD$_3$ group, collected

incubation buffers and cell lysates were spiked with deuterated internal standards d_6-25OHD$_3$-S and d_6-25OHD$_3$-G and evaporated to dryness before being derivatized with DAPTAD. For taurocholate group, incubation buffers were spiked with internal standard cholic acid and evaporated to dryness before being reconstituted in 100 µl mobile phase. The resulting samples were subject to quantification by LC-MS/MS as described below.

In the presence of calcium, the tight junctions between hepatocytes and the canalicular networks remain intact, allowing measurement of efflux across the sinusoidal membrane of hepatocytes. Removal of calcium from the incubation buffer disrupts the tight junctions and allows measurement of efflux across both the canalicular and sinusoidal membranes. Therefore, the difference in efflux between with and without calcium represents biliary efflux of a test compound. Biliary efflux index (BEI) was calculated using the equation: BEI (%) = [Efflux (sinusoidal + canalicular) – Efflux (sinusoidal)]/Efflux (sinusoidal + canalicular)] × 100.

Analytical Methods. Given simple matrix and relatively high concentrations, 25OHD$_3$-S and 25OHD$_3$-G in vesicular and cellular uptake as well as the unbound fraction determination assays were quantified using a straightforward LC-MS method reported by Wang et al. (Wang et al., 2014). As for experiments with SCHHs, due to low production of 25OHD$_3$-S and 25OHD$_3$-G in hepatocytes, 25OHD$_3$-S and 25OHD$_3$-G in the incubation buffers and cell lysates were derivatized with DAPTAD and quantified using a sensitive LC-MS/MS method as previously described (Gao et al., 2017).

E_2-17β-G in the membrane vesicular and cellular uptake assays was quantified using LC-MS with E_2-3-S as the internal standard. Briefly, chromatographic separation was achieved on a Waters Symmetry C_{18} (2.1 × 50 mm, 3.5 μm) column (Waters, Milford, MA) with a mobile phase consisting of 1 mM ammonium chloride (A) and methanol (B) at 45°C. A linear gradient from 20% B (0-0.5 min) to 75% B (4-5 min) in 3.5 min at a 0.25 mL/min flow rate was employed. The mass spectrometer was operated in the negative ionization mode. E_2-17β-G and E_2-3-S were detected by selective ion monitoring at *m/z* 447 and *m/z* 351, respectively.

E_1-3-S in the OATP2B1-overexpressing cell uptake assay was quantified using LC-MS with E_2-3-S as the internal standard. Chromatographic separation was achieved using a Waters Symmetry C_{18} (2.1 × 50 mm, 3.5 μm) column (Waters) on an Agilent 1200 LC system. The elution was performed at a flow rate of 0.25 ml/min with the mobile phase containing 0.1% formic acid in water and methanol at a ratio of 30:70 (v/v). Mass spectrometric analysis was carried out using a negative mode electrospray ionization method on an Agilent 6410 triple quadrupole tandem mass spectrometer. Single ion monitoring at *m/z* 351 and *m/z* 349 were applied for detection of E_1-3-S and E_2-3-S, respectively.

Taurocholate in SCHH efflux experiments was quantified using cholic acid as the internal standard. Chromatographic separation was achieved using a Waters Symmetry C_{18} (2.1 × 50 mm, 3.5 μm) column (Waters) on an Agilent 1200 LC system. The elution was performed at a flow rate of 0.25 ml/min with the mobile phase containing acetonitrile and 10 mM ammonium acetate (native pH) at a ratio of 64:36 (v/v). Mass spectrometric analysis was carried out using a negative

mode electrospray ionization method on an Agilent 6410 triple quadrupole tandem mass spectrometer. Single ion monitoring at *m/z* 514 and *m/z* 407 were applied for detection of taurocholate and cholic acid, respectively.

The LC-MS quantification methods for E_2-17β-G, E_1-3-S and taurocholate were developed in-house; a linear standard curve ($r^2 > 0.99$) was established for each analytical batch, and the accuracy of inter-day and intra-day quality control samples was within the range of 85-115% during the analysis.

RESULTS

Human Bile Analysis. To confirm the presence of 25OHD$_3$-S and 25OHD$_3$-G in human bile, pooled healthy human bile was derivatized with DAPTAD and analyzed using a sensitive LC-MS/MS method we developed (Gao et al., 2017). As shown in Fig. 2, peaks were observed in bile for both DAPTAD-25OHD$_3$-S (Fig. 2A) and DAPTAD-25OHD$_3$-G (Fig. 2C) at the expected slightly longer retention times as their corresponding deuterated internal standards (Fig. 2B and Fig. 2D). Based on the calibration curves established with 25OHD$_3$-S and 25OHD$_3$-G standards, concentrations of 25OHD$_3$-S and 25OHD$_3$-G in the pooled human bile were estimated to be around 2.55 nM and 0.30 nM, respectively.

ATP-dependent Uptake of 25OHD$_3$-G into Inside-out Plasma Membrane Vesicles. Detection of 25OHD$_3$-S and 25OHD$_3$-G in human bile suggests that these conjugates are likely formed in

the liver and subsequently transported to the bile via efflux transporters on the canalicular membrane of the hepatocytes. To test this possibility, we first performed a rapid screening of hepatic efflux transporters for 25OHD$_3$-S and 25OHD$_3$-G using plasma membrane vesicular transport assays. Major hepatic efflux transporters frequently reported to be involved in the efflux transport of conjugative metabolites were screened using transporter-overexpressing plasma membrane vesicles; these included MRP2 and BCRP on the hepatic canalicular membrane and MRP3 and MRP4 on the sinusoidal membrane. Statistically significant differences in uptake of 50 µM E$_2$-17β-G, a known substrate of these transporters, into plasma membrane vesicles between the ATP and AMP groups were observed with vesicles overexpressing each of the transporters (Fig. 3A). Differences between the ATP and AMP groups associated with the mock control vesicles were also significant, but much smaller than those associated with the transporter-overexpressing vesicles. Furthermore, uptake of E$_2$-17β-G into transporter-overexpression vesicles was significantly greater than that into the mock control vesicles in the presence of ATP (Fig. 3A). These data confirmed that the membrane vesicles we used were functional. By incubating 2 µM of 25OHD$_3$-G with membrane vesicles at 37ºC for 5 min, significant ATP-dependent active uptake of 25OHD$_3$-G by MRP2 and MRP3 was observed (Fig. 3B), suggesting that 25OHD$_3$-G is a substrate of these efflux transporters. On the other hand, there was no significant active uptake of 25OHD$_3$-G by BCRP and MRP4 (Fig. 3B), suggesting that 25OHD$_3$-G is not a substrate of BCRP and MRP4. To further confirm these findings, we performed inhibition studies using selective MRP inhibitors. MK571 (Weiss et al.,

DMD Fast Forward. Published on February 21, 2018 as DOI: 10.1124/dmd.117.078881
This article has not been copyedited and formatted. The final version may differ from this version.

2007) and indomethacin (Draper et al., 1997) are relatively selective inhibitors for MRP transporters. We found that the net ATP-dependent uptake of 25OHD$_3$-G at 2 µM into MRP2- and MRP3-expressing plasma membrane vesicles was significantly reduced by 50 µM of MK571 by 70% (Fig. 4A) and 50% (Fig. 4B), respectively. Indomethacin at 672 µM also significantly inhibited MRP3-mediated active uptake of 25OHD$_3$-G by ~75% (Fig. 4B). Results of the inhibition studies provided additional evidence to support the notion that 25OHD$_3$-G can be actively transported by MRP2 and MRP3. Both MK571 and indomethacin also decreased the net active uptake of 25OHD$_3$-G into Sf9 mock membrane vesicles (Fig. 4A and Fig. 4B), suggesting that Sf9 cells express low levels of endogenous MRP transporters capable of transporting 25OHD$_3$-G.

We next estimated kinetic parameters (K_m and V_{max}) for MRP2- and MRP3-mediated efflux of 25OHD$_3$-G. The representative transport kinetic profiles are shown in Fig. 4C for MRP2, and in Fig. 4D for MRP3. Given high non-specific binding of 25OHD$_3$-G which can influence kinetic parameter estimation, we first determined unbound fractions of 25OHD$_3$-G in incubation buffers used in the vesicular transport assays, and then used unbound fractions to correct K_m values. We found that the unbound fraction Y (%) of 25OHD$_3$-G exhibited a linear relation with the total concentration (X) following the equation: $Y = 0.0018X + 7.3119$ (r^2 = 0.9965) within the concentration range of 0-10 µM, and then reached saturation at ~25%. After correction with unbound fractions at respective total concentrations, the K_m values for MRP2- and MRP3-mediated transport of 25OHD$_3$-G were 1.56 ± 0.43 µM and 0.25 ± 0.04 µM, and the

DMD Fast Forward. Published on February 21, 2018 as DOI: 10.1124/dmd.117.078881
This article has not been copyedited and formatted. The final version may differ from this version.

V_{max} were 295.6 ± 87.1 pmol/mg protein/min and 66.7 ± 11.6 pmol/mg protein/min, respectively.

Inhibition of Efflux Transporter Activity by 25OHD$_3$-S. Due to high non-specific binding and passive diffusion, we noticed very high background levels associated with membrane vesicles even after extensive washing with 1.5% BSA or DBP. Such a high background appeared to completely mask activity of efflux transporters for 25OHD$_3$-S with no significant differences in the uptake into membrane vesicles between the ATP and AMP groups (data not shown). Therefore, we were unable to demonstrate whether 25OHD$_3$-S is a substrate of the efflux transporters examined including BCRP, MRP2, MRP3 and MRP4. To further evaluate the interactions of 25OHD$_3$-S with these transporters, inhibition studies using a model substrate of these transporters (E_2-17β-G) were conducted. As shown in Fig. 5, 25OHD$_3$-S effectively inhibited ATP-dependent transport of E_2-17β-G by BCRP (Fig. 5A), MRP4 (Fig. 5B), and MRP3 (Fig. 5C) in a concentration-dependent manner, suggesting that 25OHD$_3$-S is a ligand and possibly a substrate of these three transporter proteins. In contrast, 25OHD$_3$-S did not inhibit MRP2-mediated transport of E_2-17β-G at all (data not shown). We also determined unbound factions of 25OHD$_3$-S in incubation buffers of the vesicular transport assays and found that the unbound fraction of 25OHD$_3$-S was ~8% in both HEK293 and Sf9 membrane vesicles and independent of total concentration. After correction for unbound fraction, IC_{50} values of 25OHD$_3$-S for inhibition of BCRP-, MRP4- and MRP3-mediated transport of E_2-17β-G from duplicate experiments were estimated to be 1.0, 0.96 and 1.88 μM, respectively.

DMD Fast Forward. Published on February 21, 2018 as DOI: 10.1124/dmd.117.078881
This article has not been copyedited and formatted. The final version may differ from this version.

Efflux of 25OHD$_3$-S and 25OHD$_3$-G from Sandwich Cultured Human Hepatocytes.

According to results of membrane vesicular transport studies and the detection of 25OHD$_3$ conjugative metabolites in human bile as described above, we hypothesized that 25OHD$_3$-S and 25OHD$_3$-G are transported out of human hepatocytes into the bile after they are converted from 25OHD$_3$ in the liver. To test this hypothesis, we examined biliary efflux of 25OHD$_3$-S and 25OHD$_3$-G using SCHHs. Taurocholate is known to have extensive biliary efflux and therefore was used as a positive control for each preparation of SCHHs. As expected, the efflux of taurocholate from SCHHs in the absence of calcium was significantly higher than that in the presence of calcium over time for all five different batches of SCHHs we used with the exception of HH1007 at earlier time points (5 and 10 min) (Fig. 6), suggesting that SCHHs we used were functional.

After incubation of 25OHD$_3$ at 10 μM with SCHHs for 4 h, we found that 25OHD$_3$-S and 25OHD$_3$-G representing ~3% of the starting dose of 25OHD$_3$ were formed with a product formation ratio of around 30:1 (25OHD$_3$-S: 25OHD$_3$-G) calculated based on their recovery from efflux incubation buffers and cell lysates of SCHH. Both 25OHD$_3$-S and 25OHD$_3$-G rapidly appeared in the efflux buffer in the absence and presence of calcium and their concentrations increased with time, suggesting a time-dependent passive or active efflux of the conjugates from hepatocytes (Fig. 6). We noticed substantial inter-individual variations in both sinusoidal and canalicular efflux of 25OHD$_3$-S and 25OHD$_3$-G among SCHHs from five different donors. The

increases in concentrations of 25OHD$_3$-S and 25OHD$_3$-G in efflux buffers over time (0-20 min) in the presence of calcium, which represent sinusoidal efflux rates, followed the rank orders of HH1007 > HH1055 > HH1031 > HH1085 > HH1103 and of HH1055 > HH1007 > HH1103 > HH1031 > HH1085 for 25OHD$_3$-S and 25OHD$_3$-G, respectively. In the absence of calcium, concentrations of 25OHD$_3$-S in efflux buffers over time were significantly higher than those in the presence of calcium in SCHHs from donors HH1055, HH1103, HH1085 and HH1007, but not HH1031. In particular, SCHHs from the donor HH1055 showed significantly higher canalicular efflux activity of 25OHD$_3$-S than other donors. Likewise, concentrations of 25OHD$_3$-G in efflux buffers over time in the absence of calcium were significantly higher than those in the presence of calcium in SCHHs from donors HH1055, HH1085 and HH1007, but not HH1103 and HH1031. The donor HH1031 did not exhibit canalicular efflux of either 25OHD$_3$-S nor 25OHD$_3$-G, despite high canalicular efflux of taurocholate.

To confirm if BCRP or MRPs are involved in the canalicular and sinusoidal efflux of 25OHD$_3$-S and 25OHD$_3$-G, FTC, a selective BCRP inhibitor or MK571, a selective MRP inhibitor was added to incubation buffer during the loading and efflux phases. SCHHs from the donor HH1055, which showed the highest efflux activity among all the donors analyzed, were used in the inhibition studies. As expected, the canalicular efflux of 25OHD$_3$-S was significantly decreased by the addition to FTC compared to control with no FTC added. We calculated biliary efflux index (BEI) in the presence and absence of FTC. The mean BEI (%) of 25OHD$_3$-S from three independent experiments was significantly decreased by FTC at 15 min and 20 min of

efflux (Table 1), confirming that the biliary efflux of 25OHD$_3$-S is likely mediated by BCRP. However, the effects of MK571 on the efflux of 25OHD$_3$-G and 25OHD$_3$-S cannot be analyzed. Due to the near complete inhibition on both the glucuronidation and sulfation of 25OHD$_3$ in the hepatocytes by MK571 (data not shown), the two conjugative metabolites were undetectable in most of efflux buffers analyzed.

Cellular Uptake of 25OHD$_3$-G and 25OHD$_3$-S by OATPs. OATP2B1 is a major uptake transporter in the enterocytes and facilitates in intestinal absorption of xenobiotics (Tamai, 2012). Once in the bile, 25OHD$_3$-G and 25OHD$_3$-S could be excreted to the intestinal lumen and be absorbed into the enterocytes by uptake transporters. In addition, 25OHD$_3$-G and 25OHD$_3$-S in the circulation may be transported back into the hepatocytes by uptake transporters on the sinusoidal membrane, such as OATP1B1 and OATP1B3. We therefore performed cellular uptake studies to show if 25OHD$_3$-G and 25OHD$_3$-S are substrates of OATP2B1, OATP1B1 and OATP1B3. E$_1$-3-S was used as a positive control, as it is a known substrate of OATP2B1. As expected, cellular accumulation of E$_1$-3-S in Flp-In-CHO/OATP2B1 cells was approximately 10 times greater than that in mock CHO control cells (Fig. 7A). We found that cellular accumulation of 25OHD$_3$-S in Flp-In-CHO/OATP2B1 cells was significantly increased by ~50% compared to that in mock CHO cells (Fig. 7A); however, there were no significant differences in uptake of 25OHD$_3$-G into OATP2B1 cells and the mock control cells (Fig. 7A). The results indicate that 25OHD$_3$-S, but not 25OHD$_3$-G, is a substrate of OATP2B1. Further kinetic measurements

revealed an unbound K_m of 1.9 ± 0.9 μM and a V_{max} of 81.3 ± 11.8 pmol/mg protein/min for OATP2B1-mediated uptake of 25OHD$_3$-S from 5 independent experiments. A representative kinetic profile of OATP2B1-mediated uptake of 25OHD$_3$-S is shown in Fig. 7B.

Furthermore, cellular accumulation of 25OHD$_3$-S in OATP1B3-overexpressing CHO cells was about 2-fold ($p < 0.001$) of that in wild-type CHO parent cells and this difference was completely abolished by the addition of 20 μM CsA, a potent OATP inhibitor (Fig. 8A). On the other hand, there were no differences in cellular accumulation of 25OHD$_3$-S in OATP1B1-overexpressing cells and the wild-type CHO parent cells (Fig. 8A). The data indicate that 25OHD$_3$-S is a substrate of OATP1B3, but not OATP1B1. Likewise, cellular accumulation of 25OHD$_3$-G in OATP1B1- and OATP1B3-overexpressing cells was approximately 4-fold ($p < 0.001$) and 25-fold ($p < 0.001$) greater than that in the wild-type CHO parent cells, respectively, and this difference was completely diminished by CsA (Fig. 8B). Therefore, 25OHD$_3$-G is a substrate of both OATP1B1 and OATP1B3.

DISCUSSION

The present study demonstrates active transport of 25OHD$_3$-S and/or 25OHD$_3$-G by MRP2, MRP3, MRP4, BCRP, OATP1B1, OATP1B3 or OATP2B1. Due to lipophilic side chain at carbon C20, 25OHD$_3$-S and 25OHD$_3$-G were highly bound to cell membrane and plastic surface. This resulted in high background levels in membrane vesicular and cellular accumulation assays, which masked real active transport, and initially no direct uptake could be observed for either

$25OHD_3$-S or $25OHD_3$-G on our first try. To reduce non-specific binding, we optimized washing steps with a final washing buffer containing 1.5% BSA (w/v) that were repeated five and two times for membrane vesicle and intact cell, respectively. Addition of DBP offered no further advantage (data not shown). These conditions allowed us to quantify direct active uptake of $25OHD_3$-G into membrane vesicles and transfected cells, and active uptake of $25OHD_3$-S into transfected cells, but not membrane vesicles. Although we did not observe ATP-dependent transport of $25OHD_3$-S into membrane vesicles, we found that $25OHD_3$-S was a potent inhibitor of E_2-17β-G transport by BCRP, MRP3 and MRP4, indicating that $25OHD_3$-S is a ligand and possibly a substrate of these transporters.

Dehydroepiandrosterone sulfate (DHEAS) is a steroid sulfate conjugate which has a similar structure as $25OHD_3$-S, except for the lipophilic side chain at carbon C20. DHEAS has been shown to be a potent inhibitor of MRP1, MRP4 and BCRP, and a substrate of these transporters by direct vesicular uptake (Suzuki et al., 2003; Zelcer et al., 2003). Considering the similar structures of $25OHD_3$-S and DHEAS, it is plausible that they share comparable transporter binding properties. Therefore, inhibition of transporter activities by $25OHD_3$-S, which was observed in the current study, is most likely competitive in nature and $25OHD_3$-S is possibly a substrate of MRP3, MRP4 and BCRP. Whether active transport of $25OHD_3$-S is of physiological importance depends on the extent of passive diffusion *vs* non-specific sequestration in the membrane vesicle systems, something we have not been able to address at this time. The failure to show direct uptake of $25OHD_3$-S into membrane vesicles could be due to high

membrane permeability, driven by high lipophilicity (LogP: 7.386, calculated using Advanced Chemistry Development (ACD/Labs) Software V11.02) compared to DHEAS (LogP: 3.522), much smaller inner space volume of membrane vesicles compared to intact cells, as well as high levels of protein binding. These resulted in high background levels associated with membrane vesicles that could not be reduced by extensive wash with high concentrations of BSA and DBP.

To confirm biliary transport in a more physiological model, efflux of 25OHD$_3$-S and 25OHD$_3$-G were investigated in SCHHs. There are theoretically two ways to load the compounds in this system: 1) directly load 25OHD$_3$-S and 25OHD$_3$-G and determine the efflux after removing excessive free compounds; 2) incubate 25OHD$_3$ with SCHHs to generate 25OHD$_3$-S and 25OHD$_3$-G, and then observe the efflux of produced metabolites. Direct loading appears to be straightforward, time-saving, and not affected by metabolite formation activity of the hepatocyte. However, after several attempts, we found that excessive unbound conjugates from the loading step could not be sufficiently removed, even after extensive washing with BSA-containing media, to permit quantitation of net active transport. Therefore, the second method was adopted, and the conjugates were generated *de novo* from 25OHD$_3$ in SCHHs before assessment of hepatic efflux. Of course, this had the advantage of better mimicking *in vivo* hepatic disposition of the 25OHD$_3$ conjugates. We also found that it was necessary to include DPB in the efflux buffer to facilitate release of 25OHD$_3$-S and 25OHD$_3$-G from cell surface during the efflux phase, something that is also expected *in vivo* for basolateral transport. Without DBP, only minimal amount of 25OHD$_3$-S and 25OHD$_3$-G could be detected in the efflux buffer,

which is consistent with the competing affinity of 25OHD$_3$-S and 25OHD$_3$-G for cell membranes or plastic surface. However, it is difficult to predict what happens during biliary transport based on our *in vitro* observation. Bile does not contain DBP, but it is rich in bile salts, which are good surfactants, and might greatly enhance the solubility and affinity of lipophilic 25OHD$_3$-S and 25OHD$_3$-G conjugates in bile.

We observed substantial inter-individual variations of both sinusoidal and canalicular efflux of 25OHD$_3$-S and 25OHD$_3$-G in SCHHs from five different donors, which could be caused by inter-individual variations in efflux transporter expression. However, due to limitation of method sensitivity and sample amount available, quantification of protein levels of efflux transporters in the SCHHs by LC-MS-based proteomics could not be achieved (data not shown). To evaluate the roles of MRPs and BCRP in the efflux of 25OHD$_3$-S and 25OHD$_3$-G in SCHHs, relatively specific inhibitors were added to chemically knock-out the corresponding transporter. In our SCHH efflux assays, 25OHD$_3$-S and 25OHD$_3$-G were formed in hepatocytes during the 4-h loading phase with 25OHD$_3$, during which the conjugates could be effluxed into bile canaliculi immediately upon formation. Therefore, to completely block the efflux, the transporter inhibitor was added at the beginning of both loading and efflux phases. The BCRP specific inhibitor FTC significantly reduced the canalicular efflux of 25OHD$_3$-S, suggesting an essential role of BCRP in the biliary efflux of 25OHD$_3$-S from the liver. To inhibit MRPs, we used MK571, the most commonly used MRP inhibitor. However, we found that MK571 had a profound effect on the conjugative enzymes, essentially abolishing 25OHD$_3$-S and 25OHD$_3$-G

formation from 25OHD$_3$. This has also been observed by other researchers (Barrington et al., 2015). Due to low metabolic formation, the roles of MRPs in the efflux of 25OHD$_3$-S and 25OHD$_3$-G in SCHHs could not be evaluated. We recognize that the concentration of 25OHD$_3$ (10 μM) we used in experiments with SCHHs is not a physiological exposure. Lower concentrations could not be used because of analytical limitations. However, given the very long half-life of 25OHD$_3$ in humans (14 days), we would suggest that hepatic 25OHD$_3$ conjugation and biliary secretion *in vivo* is a slow but physiologically important process, even at low (50 nM) physiological concentrations of 25OHD$_3$.

The absence of 25OHD$_3$-S and 25OHD$_3$-G in urine, despite significant circulating concentrations (Wong et al., 2018), suggests that there is an effective means for hepatic reuptake of 25OHD$_3$-S and 25OHD$_3$-G. OATP1B1, OATP2B1 and OATP1B3 are the major uptake transporters on the sinusoidal membrane of hepatocytes (Badée et al., 2015). Besides the liver, OATP2B1 is also expressed in many other tissues, including intestinal epithelial cells (Gröer et al., 2013). We showed that 25OHD$_3$-S is a good substrate of OATP2B1 and OATP1B3, providing a mechanism for excretion from the body through the liver. This also offers a mechanism for intestinal absorption of 25OHD$_3$-S, followed by excretion into the bile (by BCRP). Similarly, the excretion of 25OHD$_3$-G from the body may be initiated by OATP1B1/OATP1B3-mediated hepatic uptake, followed by MRP2-mediated biliary excretion. Although 25OHD$_3$-G was not transported by OATP2B1, it might be deconjugated by the intestinal bacteria, which are rich in glucuronidase and can hydrolyze diverse types of

DMD Fast Forward. Published on February 21, 2018 as DOI: 10.1124/dmd.117.078881
This article has not been copyedited and formatted. The final version may differ from this version.

glucuronide conjugates (Kim and Jin, 2001; Gao et al., 2011). Generated $25OHD_3$ could then be reabsorbed from the intestinal lumen by passive diffusion.

Considering that $25OHD_3$-S (Wong et al., 2018) and $25OHD_3$-G (Wang et al., 2014) are strongly bound to DBP and that DBP is produced in the liver, it is possible that the conjugates formed in the liver could also be effluxed into blood out of the liver bound to the DBP, following protein synthesis in the liver. This mechanism was postulated for other lipophilic vitamins, such as vitamin E (Drevon, 1991) and vitamin K (Shearer et al., 2012), which are transported out of the liver bound to lipoproteins. Whether this occurs for $25OHD_3$ conjugates is unknown and remains to be investigated.

In summary, as shown in Fig. 9, the present study revealed that $25OHD_3$-G is a substrate of MRP2, MRP3, OATP1B1 and OATP1B3, and that $25OHD_3$-S is a substrate of OATP2B1 and OATP1B3, and possibly a substrate of BCRP, MRP3 and MRP4. Thus, in the liver, $25OHD_3$-G and $25OHD_3$-S could be excreted into the bile though MRP2 and BCRP, respectively, and back into the blood circulation by MRP3 (both) and MRP4 ($25OHD_3$-S). The sinusoidal OATP transporters may pump unbound $25OHD_3$-G and $25OHD_3$-S from the blood into hepatocytes for further biliary excretion or blood recirculation. In the intestinal tract, OATP2B1 may mediate transport of $25OHD_3$-S into proximal enterocytes, following biliary excretion. Parts of the model presented in Fig. 9 related to the intestinal disposition and downstream effects of $25OHD_3$-G and $25OHD_3$-S are speculative and not yet supported by experimental evidence. We present it to stimulate further research and hypothesis testing. For example, can $25OHD_3$-S and $25OHD_3$-G

be deconjugated to $25OHD_3$ by intestinal sulfatases or glucuronidases? Would this occur in the lumen of the gastrointestinal traction or after transporter mediated uptake into enterocytes? What is the kinetics of $25OHD_3$ metabolism to $1\alpha,25\text{-}(OH)_2D_3$ by CYP27B1 in the intestinal tract and would in vivo conversion rates enhance enterocyte levels of $1\alpha,25\text{-}(OH)_2D_3$ following biliary secretion of $25OHD_3$ conjugates? Lastly, the relative importance of the conjugative pathways versus the oxidation pathways (shown in Fig. 1) in the systemic clearance of $25OHD_3$ remains unclear, as is the contribution of enterohepatic circulation of the $25OHD_3$ conjugates to the overall disposition and biological activity of vitamin D. These are important topics of future investigation and the present study represents the first step in addressing this knowledge gap.

ACKNOWLEDGEMENTS

We would like to thank Dr. Danny D. Shen and Brian R. Phillips in the Department of Pharmaceutics, University of Washington, Seattle, for sharing LC-MS instruments and assistance in the analytical method development. We also greatly thank Drs. Bruno Stieger and Bruno Hagenbuch for their generous gifts of cell lines.

AUTHORSHIP CONTRIBUTIONS

Participated in research design: Gao, Thummel and Mao

Conducted experiments: Gao, Liao and Han

Performed data analysis: Gao

Wrote or contributed to the writing of the manuscript: Gao, Liao, Han, Thummel and Mao

REFERENCES

Arnaud SB, Goldsmith RS, Lambert PW, and Go VL (1975) 25-Hydroxyvitamin D3: evidence of an enterohepatic circulation in man. Proceedings of the Society for Experimental Biology and Medicine 149:570-572.

Avioli LV, Lee SW, McDonald JE, Lund J, and DeLuca HF (1967) Metabolism of vitamin D3-3H in human subjects: distribution in blood, bile, feces, and urine. Journal of Clinical Investigation 46:983-992.

Badée J, Achour B, Rostami-Hodjegan A, and Galetin A (2015) Meta-Analysis of Expression of Hepatic Organic Anion–Transporting Polypeptide (OATP) Transporters in Cellular Systems Relative to Human Liver Tissue. Drug Metabolism and Disposition 43:424-432.

Balesaria S, Sangha S, and Walters JR (2009) Human duodenum responses to vitamin D metabolites of TRPV6 and other genes involved in calcium absorption. American Journal of Physiology-Gastrointestinal and Liver Physiology 297:G1193-G1197.

Barrington RD, Needs PW, Williamson G, and Kroon PA (2015) MK571 inhibits phase-2 conjugation of flavonols by Caco-2/TC7 cells, but does not specifically inhibit their apical efflux. Biochemical pharmacology 95:193-200.

Bikle DD (2009) Extra renal synthesis of 1, 25-dihydroxyvitamin D and its health implications. Clinical Reviews in Bone and Mineral Metabolism 7:114-125.

Bikle DD (2014) Vitamin D metabolism, mechanism of action, and clinical applications. Chemistry & biology 21:319-329.

Bises G, Kállay E, Weiland T, Wrba F, Wenzl E, Bonner E, Kriwanek S, Obrist P, and Cross HS (2004) 25-hydroxyvitamin D3-1α-hydroxylase expression in normal and malignant human colon. Journal of Histochemistry & Cytochemistry 52:985-989.

Christakos S (2012) Mechanism of action of 1, 25-dihydroxyvitamin D3 on intestinal calcium absorption. Reviews in Endocrine and Metabolic Disorders 13:39-44.

Christakos S, Ajibade DV, Dhawan P, Fechner AJ, and Mady LJ (2010) Vitamin D: metabolism. Endocrinology and metabolism clinics of North America 39:243-253.

Draper M, Martell R, and Levy S (1997) Indomethacin-mediated reversal of multidrug resistance and drug efflux in human and murine cell lines overexpressing MRP, but not P-glycoprotein. British Journal of Cancer 75:810-815.

Drevon CA (1991) Absorption, transport and metabolism of vitamin E. Free radical research communications 14:229-246.

Duan H, Hu T, Foti RS, Pan Y, Swaan PW, and Wang J (2015) Potent and selective inhibition of plasma membrane monoamine transporter by HIV protease inhibitors. Drug Metabolism and Disposition 43:1773-1780.

Feldman D, Krishnan AV, Swami S, Giovannucci E, and Feldman BJ (2014) The role of vitamin D in reducing cancer risk and progression. Nature reviews cancer 14:342-357.

Gao C, Bergagnini-Kolev MC, Liao MZ, Wang Z, Wong T, Calamia JC, Lin YS, Mao Q, and Thummel KE (2017) Simultaneous quantification of 25-hydroxyvitamin D3-3-sulfate and 25-hydroxyvitamin D3-3-glucuronide in human serum and plasma using liquid chromatography–tandem mass spectrometry coupled with DAPTAD-derivatization. Journal of Chromatography B 1060:158-165.

Gao C, Chen X, and Zhong D (2011) Absorption and disposition of scutellarin in rats: A pharmacokinetic explanation for the high exposure of its isomeric metabolite. Drug Metabolism and Disposition 39:2034-2044.

Gao C, Zhang H, Guo Z, You T, Chen X, and Zhong D (2012a) Mechanistic studies on the absorption and disposition of scutellarin in humans: selective OATP2B1-mediated hepatic uptake is a likely key determinant for its unique pharmacokinetic characteristics. Drug Metabolism and Disposition 40:2009-2020.

Gao R, Li L, Xie C, Diao X, Zhong D, and Chen X (2012b) Metabolism and pharmacokinetics of morinidazole in humans: identification of diastereoisomeric morpholine N+-glucuronides catalyzed by UDP glucuronosyltransferase 1A9. Drug Metabolism and Disposition 40:556-567.

Gawlik A, Gepstein V, Rozen N, Dahan A, Ben-Yosef D, Wildbaum G, Verbitsky O, Shaoul R,

Weisman Y, and Tiosano D (2015) Duodenal expression of 25 hydroxyvitamin D3-1α-hydroxylase is higher in adolescents than in children and adults. The Journal of Clinical Endocrinology & Metabolism 100:3668-3675.

Gröer C, Brück S, Lai Y, Paulick A, Busemann A, Heidecke C, Siegmund W, and Oswald S (2013) LC–MS/MS-based quantification of clinically relevant intestinal uptake and efflux transporter proteins. Journal of pharmaceutical and biomedical analysis 85:253-261.

Gui C, Obaidat A, Chaguturu R, and Hagenbuch B (2010) Development of a cell-based high-throughput assay to screen for inhibitors of organic anion transporting polypeptides 1B1 and 1B3. Current chemical genomics 4:1-8.

Henry HL and Norman AW (1984) Vitamin D: metabolism and biological actions. Annual review of nutrition 4:493-520.

Hewison M, Burke F, Evans KN, Lammas DA, Sansom DM, Liu P, Modlin RL, and Adams JS (2007) Extra-renal 25-hydroxyvitamin D 3-1α-hydroxylase in human health and disease. The Journal of steroid biochemistry and molecular biology 103:316-321.

Hofmann AF (2011) Enterohepatic circulation of bile acids. Comprehensive Physiology:567–596.

Holick MF (2007) Vitamin D deficiency. New England Journal of Medicine 357:266-281.

Kim D-H and Jin Y-H (2001) Intestinal bacterial β-glucuronidase activity of patients with colon cancer. Archives of pharmacal research 24:564-567.

Miki Y, Nakata T, Suzuki T, Darnel AD, Moriya T, Kaneko C, Hidaka K, Shiotsu Y, Kusaka H, and Sasano H (2002) Systemic distribution of steroid sulfatase and estrogen sulfotransferase in human adult and fetal tissues. The Journal of Clinical Endocrinology & Metabolism 87:5760-5768.

Oleson L and Court MH (2008) Effect of the β-glucuronidase inhibitor saccharolactone on glucuronidation by human tissue microsomes and recombinant UDP-glucuronosyltransferases. Journal of Pharmacy and Pharmacology 60:1175-1182.

Pacyniak E, Roth M, Hagenbuch B, and Guo GL (2010) Mechanism of polybrominated diphenyl ether uptake into the liver: PBDE congeners are substrates of human hepatic OATP

transporters. Toxicological Sciences 115:344-353.

Schwartz J (2009) Effects of Vitamin D Supplementation in Atorvastatin‐Treated Patients: A New Drug Interaction With an Unexpected Consequence. Clinical Pharmacology & Therapeutics 85:198-203.

Shearer MJ, Fu X, and Booth SL (2012) Vitamin K nutrition, metabolism, and requirements: current concepts and future research. Advances in Nutrition: An International Review Journal 3:182-195.

Shirasaka Y, Sager JE, Lutz JD, Davis C, and Isoherranen N (2013) Inhibition of CYP2C19 and CYP3A4 by omeprazole metabolites and their contribution to drug-drug interactions. Drug Metabolism and Disposition 41:1414-1424.

Suzuki M, Suzuki H, Sugimoto Y, and Sugiyama Y (2003) ABCG2 transports sulfated conjugates of steroids and xenobiotics. Journal of Biological Chemistry 278:22644-22649.

Tamai I (2012) Oral drug delivery utilizing intestinal OATP transporters. Advanced drug delivery reviews 64:508-514.

Thirumaran RK, Lamba JK, Kim RB, Urquhart BL, Gregor JC, Chande N, Fan Y, Qi A, Cheng C, and Thummel KE (2012) Intestinal CYP3A4 and midazolam disposition in vivo associate with VDR polymorphisms and show seasonal variation. Biochemical pharmacology 84:104-112.

Thummel KE, Brimer C, Yasuda K, Thottassery J, Senn T, Lin Y, Ishizuka H, Kharasch E, Schuetz J, and Schuetz E (2001) Transcriptional control of intestinal cytochrome P-4503A by 1α, 25-dihydroxy vitamin D3. Molecular Pharmacology 60:1399-1406.

Wang Z, Lin YS, Zheng XE, Senn T, Hashizume T, Scian M, Dickmann LJ, Nelson SD, Baillie TA, and Hebert MF (2012) An inducible cytochrome P450 3A4-dependent vitamin D catabolic pathway. Molecular pharmacology 81:498-509.

Wang Z, Wong T, Hashizume T, Dickmann LZ, Scian M, Koszewski NJ, Goff JP, Horst RL, Chaudhry AS, Schuetz EG, and Thummel KE (2014) Human UGT1A4 and UGT1A3 conjugate 25-hydroxyvitamin D3: metabolite structure, kinetics, inducibility, and

interindividual variability. Endocrinology 155:2052-2063.

Weiss J, Theile D, Ketabi-Kiyanvash N, Lindenmaier H, and Haefeli WE (2007) Inhibition of MRP1/ABCC1, MRP2/ABCC2, and MRP3/ABCC3 by nucleoside, nucleotide, and non-nucleoside reverse transcriptase inhibitors. Drug metabolism and disposition 35:340-344.

Whiting JF, Narciso J, Chapman V, Ransil B, Swank R, and Gollan J (1993) Deconjugation of bilirubin-IX alpha glucuronides: a physiologic role of hepatic microsomal beta-glucuronidase. Journal of Biological Chemistry 268:23197-23201.

Wong T, Wang Z, Chapron BD, Suzuki M, Claw KG, Gao C, Foti RS, Prasad B, Chapron A, Calamia J, Chaudhry A, Schuetz EG, Horst RL, Mao Q, Boer IHd, Thornton TA, and Thummel KE (2018) Polymorphic Human Sulfotransferase 2A1 Mediates the Formation of 25-Hydroxyvitamin D3-3-O-sulfate, A Major Circulating Vitamin D Metabolite in Humans. Drug Metabolism and Disposition:dmd. 117.078428.

Zelcer N, Glen R, Wielinga P, Annemieke K, van der Heijden I, Schuetz JD, and Borst P (2003) Steroid and bile acid conjugates are substrates of human multidrug-resistance protein (MRP) 4 (ATP-binding cassette C4). Biochemical Journal 371:361-367.

FOOTNOTES

This work was supported by the National Institutes of Health [grant number GM063666].

FIGURE LEGENDS

Figure 1. Major metabolic pathways of vitamin D_3 in humans.

Figure 2. MRM chromatograms of DAPTAD-derivatized 25OHD_3-S and 25OHD_3-G in human bile. Shown are multiple reaction monitoring chromatograms of DAPTAD-25OHD_3-S (**A**), DAPTAD-d_6-25OHD_3-S (**B**), DAPTAD-25OHD_3-G (**C**) and DAPTAD-d_6-25OHD_3-G (**D**) in pooled human bile from healthy subjects.

Figure 3. Screening for ATP-dependent Uptake of E_2-17β-G and 25OHD_3-G in Plasma Membrane Vesicles Overexpressing Efflux Transporters. (**A**) E_2-17β-G, a positive control substrate, was incubated at 50 µM with plasma membrane vesicles overexpressing MRP2, MRP3, BCRP and MRP4 as well as their corresponding mock control membranes at 37ºC for 5 min. (**B**) 25OHD_3-G was incubated at 2 µM with plasma membrane vesicles overexpressing MRP2, MRP3, BCRP and MRP4 as well as their corresponding mock control membranes at 37ºC for 5 min. Data shown are means ± SD of triplicate determinations in a single experiment. Differences between the ATP and AMP groups and between the transporter-overexpression and the Mock (Sf9 or HEK) groups for each transporter were analyzed the Student's *t*-test and differences with *p* values of < 0.05 were considered statistically significant. * indicates $p < 0.05$; ** indicates $p < 0.01$; *** indicates $p < 0.001$.

Figure 4. ATP-dependent Uptake of 25OHD$_3$-G into Sf9 Insect Cell Plasma Membrane Vesicles Overexpressing MRP2 and MRP3. (**A**) 25OHD$_3$-G at 10 µM was incubated with MRP2-overexpressing Sf9 plasma membrane vesicles or mock control membrane vesicles in the presence or absence of 50 µM MK571 at 37ºC for 5 min. (**B**) 25OHD$_3$-G at 3 µM was incubated with MRP3-overexpressing Sf9 plasma membrane vesicles or mock control membrane vesicles in the presence or absence of 50 µM MK571 or 672 µM indomethacin at 37ºC for 5 min. Differences between the ATP and AMP groups (net ATP-dependent uptake) were calculated and compared between the MK571 or indomethacin and vehicle (DMSO) treatments for statistical significance by the Student's *t*-test. Data shown are means ± SD of three independent experiments. * and ** indicate $p < 0.05$ and $p < 0.01$, respectively. Representative kinetic profiles of MRP2- and MRP3-mediated ATP-dependent uptake of 25OHD$_3$-G into Sf9 plasma membrane vesicles are shown in panels **C** and **D**, respectively. 25OHD$_3$-G of varying concentrations was incubated with membrane vesicles in the presence of ATP or AMP at 37ºC for 5 min. The ATP-dependent net uptake into membrane vesicles was plotted against unbound concentrations of 25OHD$_3$-G in the incubations. Data shown are means ± SD of triplicate determinations in a single experiment. Unbound K_m and V_{max} were calculated and presented as means ± SD of three independent experiments each with triplicate determinations.

Figure 5. 25OHD$_3$-S Inhibits ATP-dependent Uptake of E$_2$-17β-G into Plasma Membrane Vesicles Overexpressing BCRP, MRP4 and MRP3. Shown are representative inhibition

profiles of $25OHD_3$-S for ATP-dependent uptake of E_2-17β-G into plasma membrane vesicles overexpressing BCRP (**A**), MRP4 (**B**) and MRP3 (**C**) that were incubated with $25OHD_3$-S and E_2-17β-G at 37ºC for 5 min. In the incubation, E_2-17β-G was at 2 µM for MRP3 and 10 µM for BCRP and MRP4. ATP-dependent net uptake of E_2-17β-G (differences between the ATP and AMP groups) was plotted against log10 values of unbound concentrations of $25OHD_3$-S in membrane vesicle incubations. Data shown are means ± SD of triplicate determinations in a single experiment. Unbound IC_{50} values were estimated from two independent experiments with triplicate determinations in each experiment.

Figure 6. Efflux of $25OHD_3$-S, $25OHD_3$-G and Taurocholate from Sandwich Cultured Human Hepatocytes (SCHHs). SCHHs from 5 different donors (HH1055, HH1103, HH1031, HH1085 and HH1007) were incubated at 37°C with 10 µM $25OHD_3$ for 4 h or 2 µM taurocholate for 20 min. Efflux of $25OHD_3$-S (**A**), $25OHD_3$-G (**B**) or taurocholate (**C**) was then initiated by replacing culture media with Ca^{2+}-containing (sinusoidal efflux, filled circles) or Ca^{2+}-free (sinusoidal + canalicular efflux, open circles) HBSS. Human vitamin D binding protein (3 µM) was added to the incubation buffer during the efflux phase of $25OHD_3$. Data shown are means ± SD for quadruplicate determinations in a single experiment. Differences between with (filled circles) and without (open circles) calcium which represent the canalicular efflux were analyzed by the Student's *t*-test. *, ** and *** indicate $p < 0.05$, $p < 0.01$ and $p < 0.001$, respectively.

Figure 7. Uptake of 25OHD$_3$-S and 25OHD$_3$-G by OATP2B1. (**A**) 10 μM of 25OHD$_3$-S or 25OHD$_3$-G or 10 μM of E$_1$-3-S was incubated with OATP2B1-overexpressing or mock control CHO cells at 37 °C for 5 min. Differences in cellular accumulation of 25OHD$_3$-S, 25OHD$_3$-G or E$_1$-3-S between OATP2B1-transfected and non-transfected cells were analyzed by the Student's *t*-test. * and ** indicate $p < 0.05$ and $p < 0.01$, respectively. Data shown are means ± SD of three determinations in a single experiment. Consistent results were obtained in another two independent experiments. (**B**) A representative kinetic profile of OATP2B1-mediated uptake of 25OHD$_3$-S by OATP2B1. Net uptake was calculated by subtracting cellular accumulation of 25OHD$_3$-S in mock control cells from that in OATP2B1-overexpressing cells and plotted against unbound concentrations of 25OHD$_3$-S in incubation buffers. Data shown are means ± SD of triplicate determinations in a single experiment. K_m and V_{max} were estimated from five independent experiments with triplicate determinations in each experiment.

Figure 8. Uptake of 25OHD$_3$-S and 25OHD$_3$-G by OATP1B1 and OATP1B3. 25OHD$_3$-S (**A**) or 25OHD$_3$-G (**B**) at 2 μM was incubated with CHO/OATP1B1, CHO/OATP1B3 or wild-type (WT) parent control CHO cells at 37 °C for 5 min in the presence or absence of CsA at 20 μM. Differences in cellular accumulation of 25OHD$_3$-S (**A**) or 25OHD$_3$-G (**B**) between OATP-overexpressing cells and wild-type parent control cells were analyzed by the Student's *t*-test. ** and *** indicate $p < 0.01$ and $p < 0.001$, respectively. Data shown are means ± SD of

four determinations in a single experiment. Consistent results were obtained in another two independent experiments.

Figure 9. A Proposed Model of Enterohepatic Transport of 25OHD$_3$-S and 25OHD$_3$-G in the Liver and Intestine. Solid lines represent confirmed routes, while dash lines represent the routes to be confirmed in future studies.

DMD Fast Forward. Published on February 21, 2018 as DOI: 10.1124/dmd.117.078881
This article has not been copyedited and formatted. The final version may differ from this version.

TABLE 1. Biliary Excretion Index (BEI) of 25OHD$_3$-S in SCHHs in the Presence and Absence of the BCRP inhibitor FTC. SCHHs were incubated at 37 °C with 25OHD$_3$ (10 μM) for 4 h in the presence or absence of FTC (10 μM) and the efflux was initiated by replacing the culture media with Ca^{2+}-containing (sinusoidal efflux) or Ca^{2+}-free (sinusoidal + canalicular efflux) HBSS in the presence or absence of FTC (10 μM). Human vitamin D binding protein (3 μM) was added during the efflux phase. Data shown are means ± SD of three independent experiments, and each experiment was performed in quadruplicate. Differences between the control and FTC-inhibited groups were analyzed by the Student's *t*-test. * indicates differences with *p* values of <0.05 that were considered statistically significant.

Time (min)	BEI (%)	
	Control	FTC
10	18.3 ± 12.4	11.1 ± 11.9
15	30.8 ± 12.2	7.1 ± 4.3*
20	27.6 ± 7.5	11.9 ± 2.3*

Fig. 1

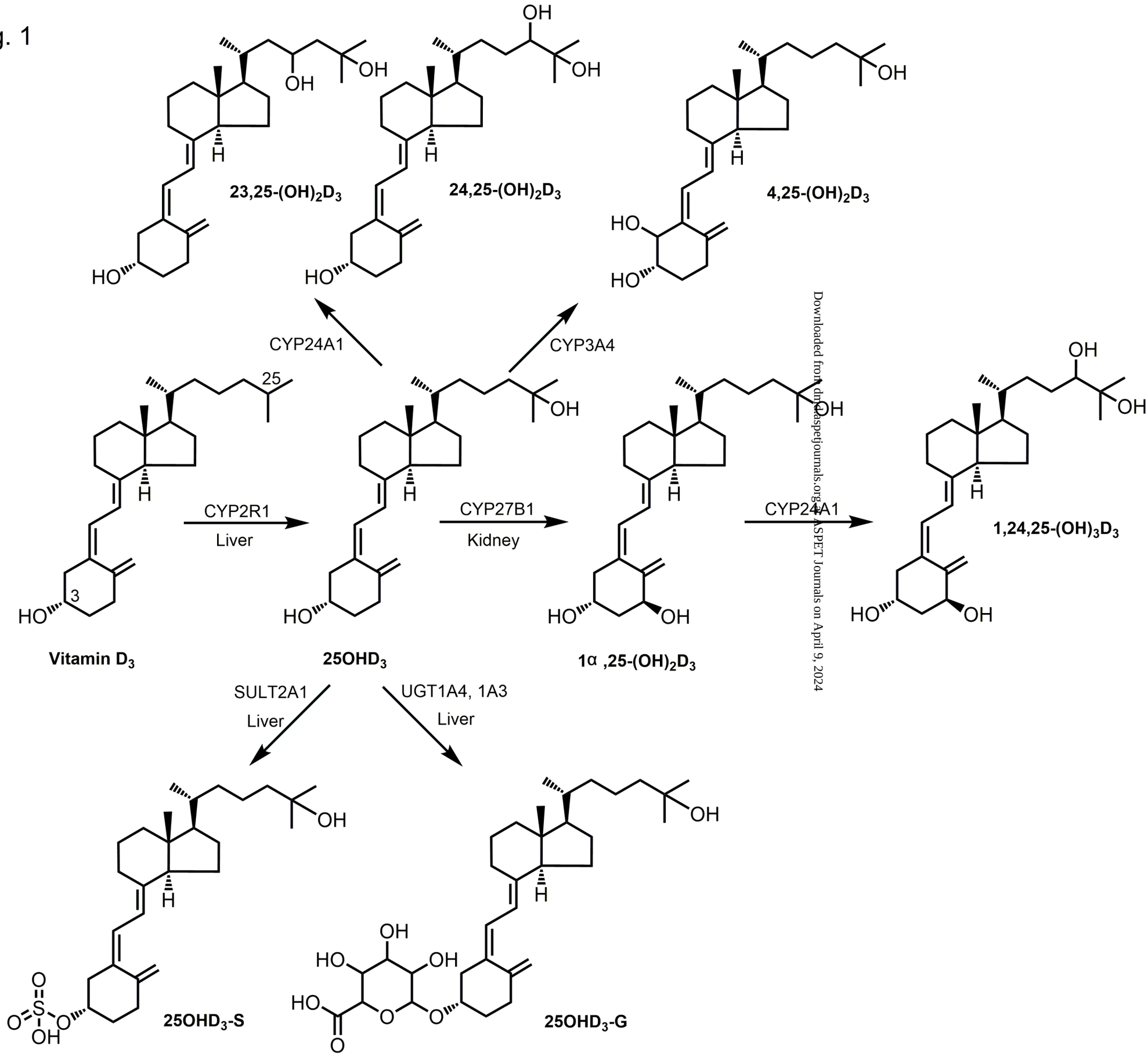

Fig. 2

DMD Fast Forward. Published on February 21, 2018 as DOI: 10.1124/dmd.117.078881
This article has not been copyedited and formatted. The final version may differ from this version.

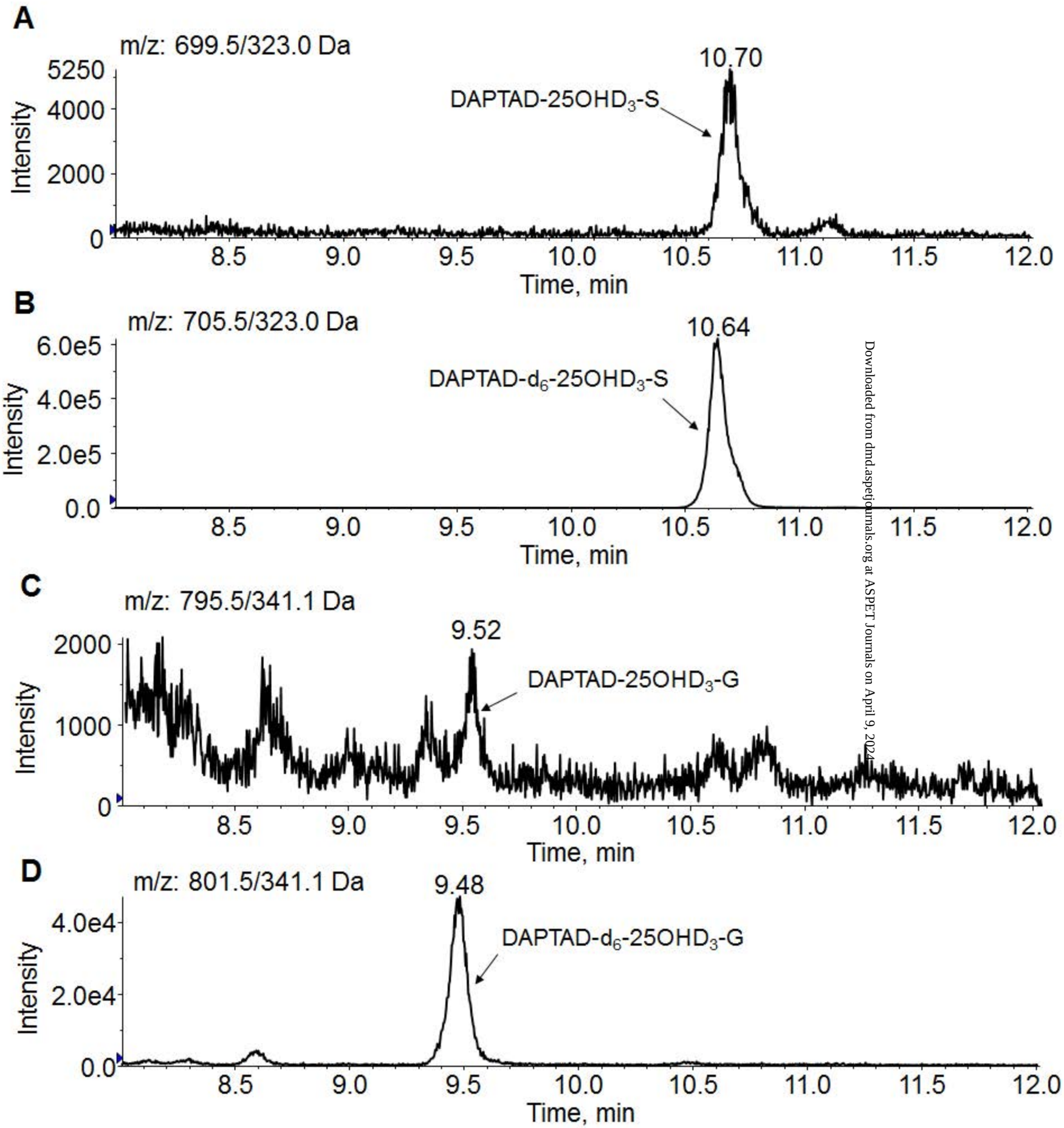

Fig. 3

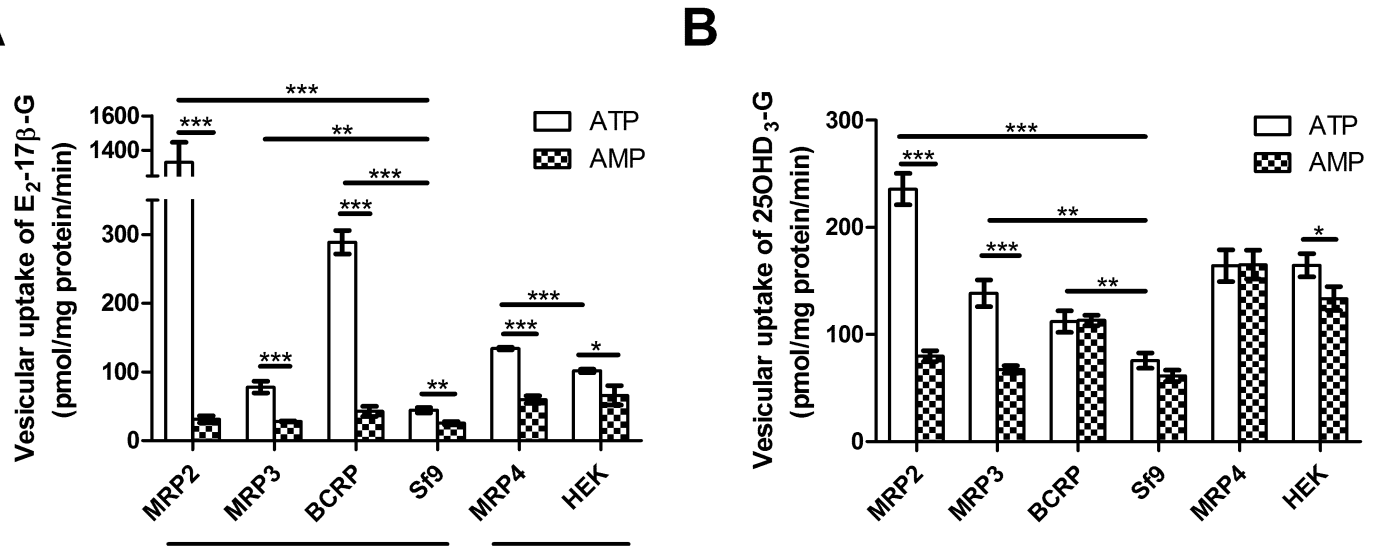
A
B
Vesicular uptake of E2-17β-G (pmol/mg protein/min)
Vesicular uptake of 25OHD3-G (pmol/mg protein/min)
ATP
AMP
MRP2
MRP3
BCRP
Sf9
MRP4
HEK
***
**
*

Fig. 4

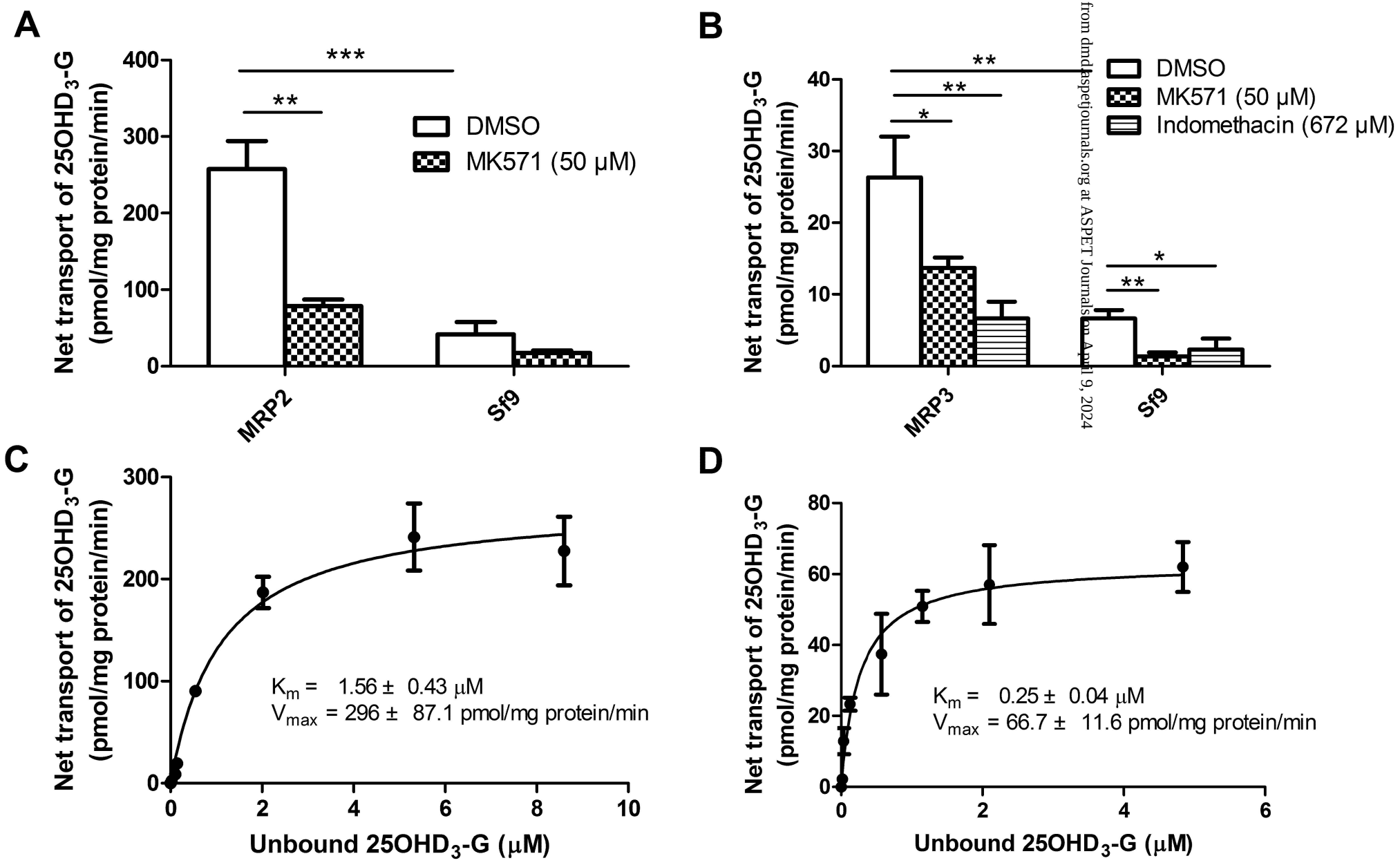

Fig. 5

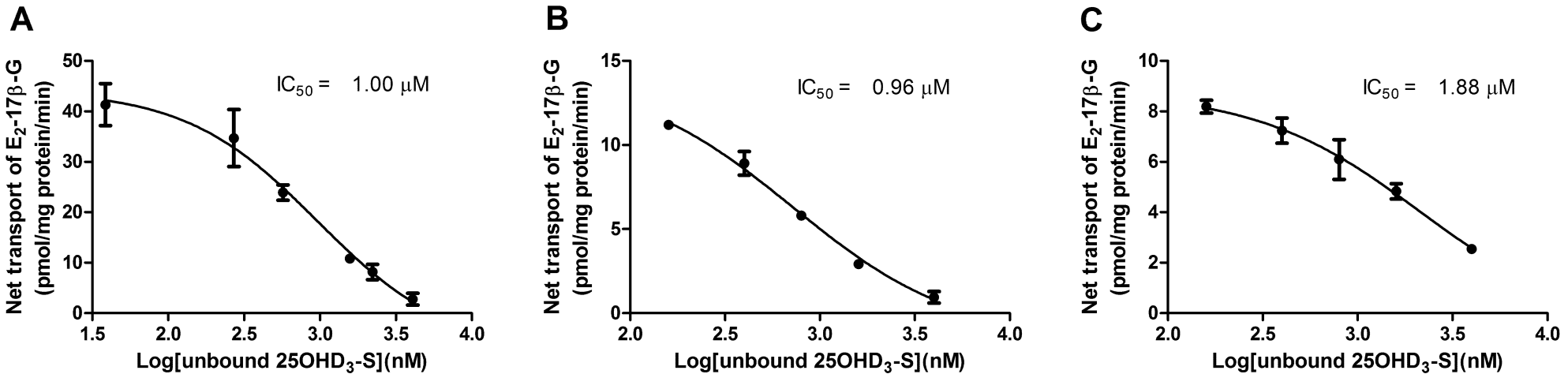
A
B
C
Net transport of E_2-17β-G (pmol/mg protein/min)
IC_{50} = 1.00 μM
IC_{50} = 0.96 μM
IC_{50} = 1.88 μM
Log[unbound 25OHD_3-S](nM)

Fig. 6

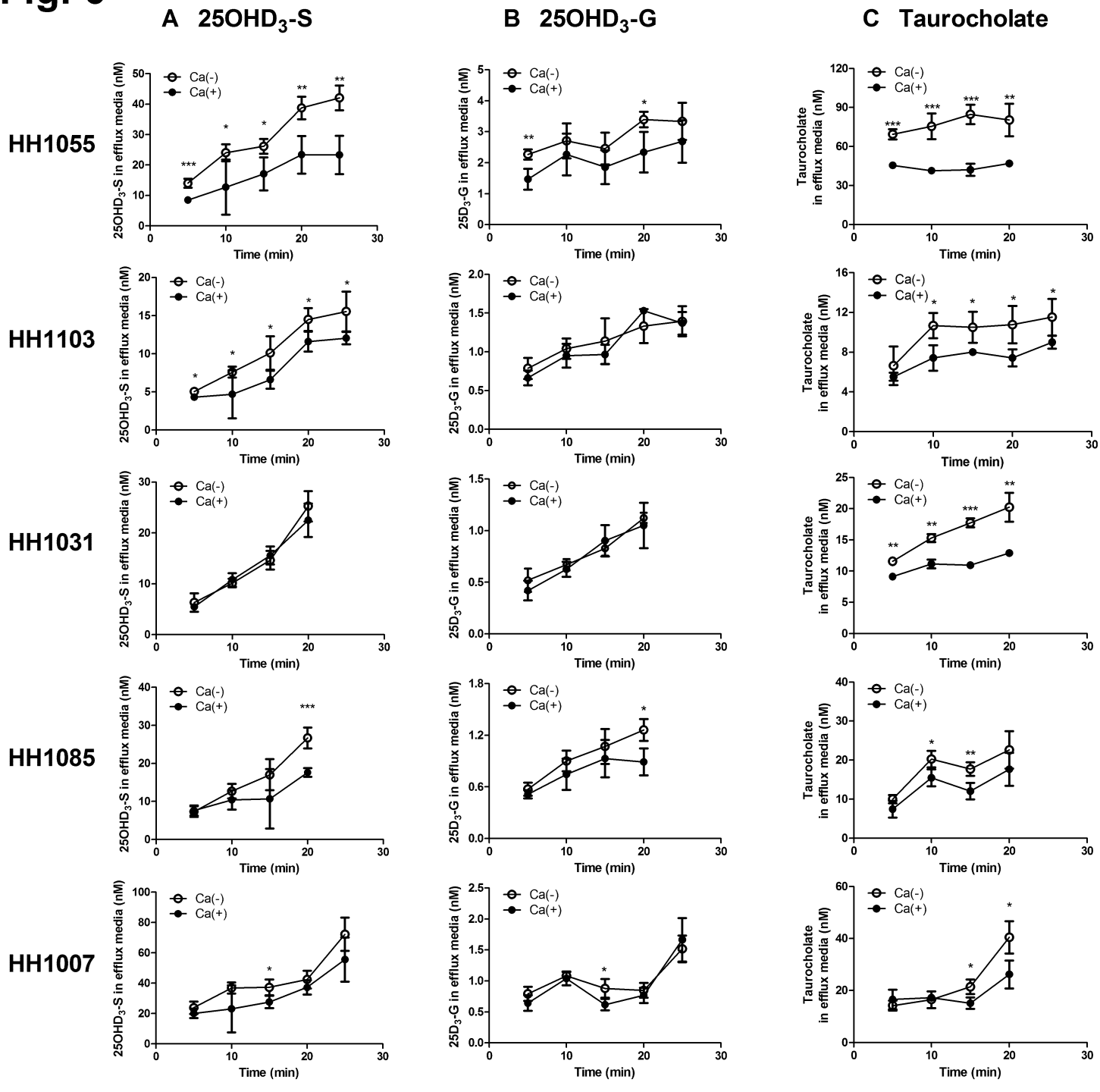
A 25OHD3-S
B 25OHD3-G
C Taurocholate
HH1055
HH1103
HH1031
HH1085
HH1007
25OHD3-S in efflux media (nM)
25D3-G in efflux media (nM)
Taurocholate in efflux media (nM)
Time (min)
Ca(-)
Ca(+)

Fig. 7

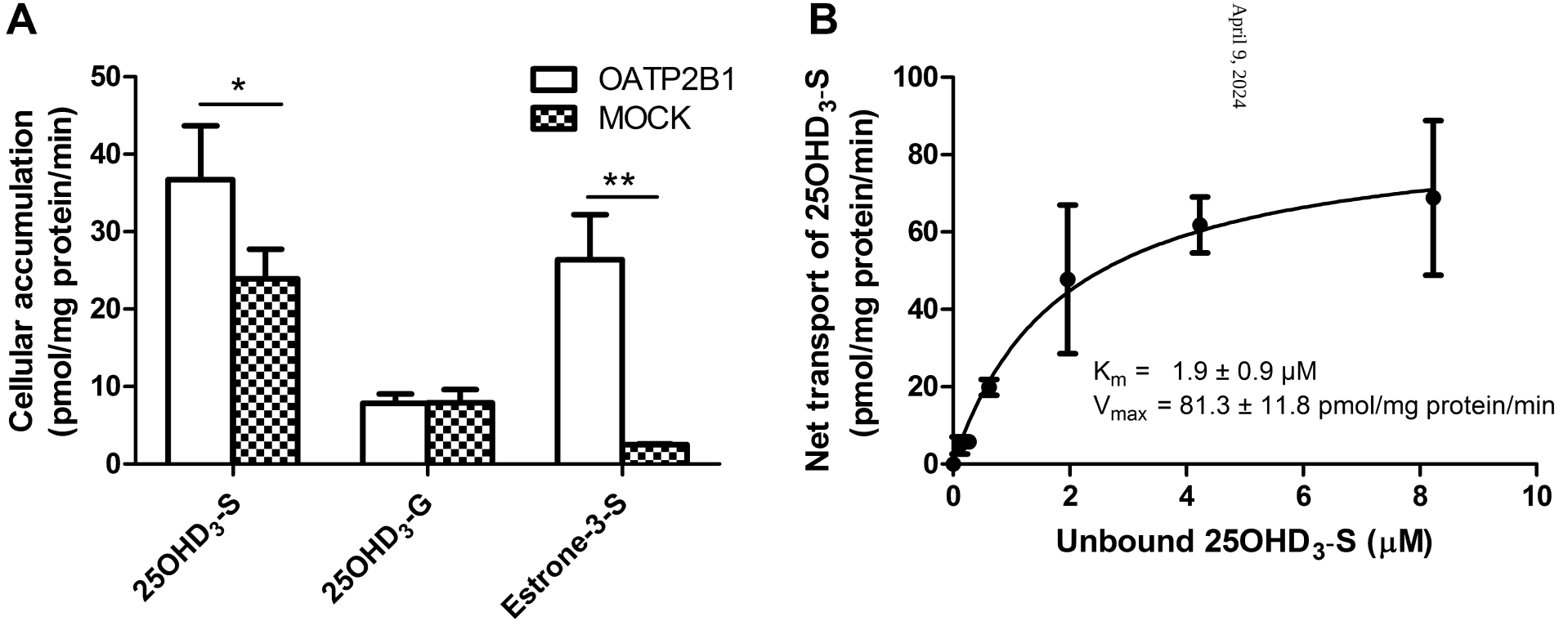

Fig. 8

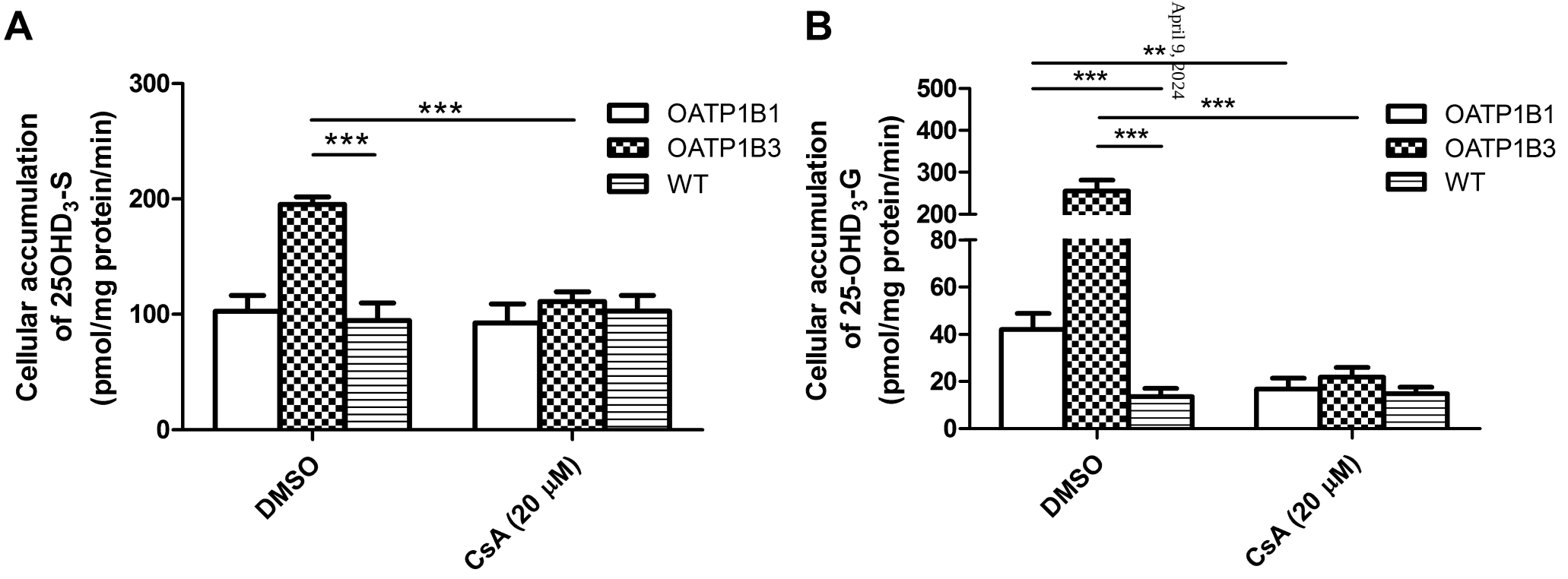

Fig. 9